




Article

Varactor-Based Tunable Sensor for Dielectric Measurements of Solid and Liquid Materials

Waseem Shahzad ^{1,*} , Weidong Hu ^{1,2,*}, Qasim Ali ¹ , Ali Raza Barket ¹  and Gulab Shah ³

¹ School of Integrated Circuits and Electronics, Beijing Institute of Technology, Beijing 100081, China; qasimali@bit.edu.cn (Q.A.); 3820182032@bit.edu.cn (A.R.B.)

² Tangshan Research Institute, Beijing Institute of Technology, Tangshan 063611, China

³ School of Information and Electronics, Nanjing University of Aeronautics and Astronautics, Nanjing 210016, China; gulab7@gmail.com

* Correspondence: waseem@bit.edu.cn (W.S.); hoowind@bit.edu.cn (W.H.)

Abstract: In this article, a tunable RF sensor is presented for the measurement of dielectric materials (liquids and solids) based on a metamaterial resonator. The proposed novel configuration sensor has a microstrip line-loaded metamaterial resonator with tunable characteristics by utilizing a single varactor diode in the series of the resonator. CST Microwave studio is employed for 3D simulations of the tunable sensor, and the desired performance is attained by optimizing various structural parameters to enhance the transmission coefficient (S_{21} magnitude) notch depth performance. The proposed RF sensor can be tuned in L and S-bands using the varactor diode biasing voltage range of 0–20 V. To validate the performance of the sensor, the proposed design has been simulated, fabricated, and tested for the dielectric characterization of different solid and liquid materials. Material testing is performed in the bandwidth of 1354 MHz by incorporating a single metamaterial resonator-based sensor. Agilent's Network Analyzer is used for measuring the S-parameters of the proposed sensor topology under loaded and unloaded conditions. Simulated and measured S-parameter results correspond substantially in the 1.79 to 3.15 GHz frequency band during the testing of the fabricated sensor. This novel tunable resonator design has various applications in modulators, phase shifters, and filters as well as in biosensors for liquid materials.



Citation: Shahzad, W.; Hu, W.; Ali, Q.; Barket, A.R.; Shah, G. Varactor-Based Tunable Sensor for Dielectric Measurements of Solid and Liquid Materials. *J. Sens. Actuator Netw.* **2024**, *13*, 8. <https://doi.org/10.3390/jsan13010008>

Academic Editor: Lei Shu

Received: 9 November 2023

Revised: 28 December 2023

Accepted: 28 December 2023

Published: 18 January 2024



Copyright: © 2024 by the authors. Licensee MDPI, Basel, Switzerland. This article is an open access article distributed under the terms and conditions of the Creative Commons Attribution (CC BY) license (<https://creativecommons.org/licenses/by/4.0/>).

Keywords: permittivity measurement; metamaterial; tunable sensor; varactor diode; square resonator

1. Introduction

One of the most significant physical aspects of dielectric materials is their dielectric properties, which demonstrate their electrical characteristic behaviors while confronted with external electromagnetic fields. The accurate assessment of the permittivity of materials is critical in many fields, including the food industry, farming, and the medical field [1–3]. There are various ways for measuring a dielectric constant of a material, including the coaxial method, resonant cavity method, waveguide technique, planar sensors, and free space method [4–7]. Planar sensors have resonant structures, which are also needed for a variety of applications in the microwave sector. Resonant structures that are of excellent quality, reliable, low profile, and lightweight are frequently used in the space and communication industries, too. Planar sensors employ resonators and are chosen among these methods for dielectric measurements due to low cost, reduced size, and light weight.

Metamaterial biosensors are also an important sensor among these types of electromagnetic sensors, which can be used to determine liquids' dielectric properties. Metamaterial sensors are advantageous compared to other sensors due to their high accuracy, high sensitivity, low cost of implementation, and easy integration to integrated circuits. In fact, these sensors can measure even a small change in the liquid dielectric properties label-free. Several different types of structures [8,9] are used in the RF band for various biomed-

cal applications also, like DNA sensing [10], in which DNA sensing is performed with a microwave regime using just a split-ring resonator.

Planar sensors can be made by using several types of resonant structures, like rings, split-ring resonators (SRRs), and complementary split-ring resonators (CSRRs) for the dielectric measurement of solids as well as liquids [9,11–13]. Planar structures have transmission lines, like microstrip lines (MTLs) or co-planar waveguides (CPWs) coupled to these resonators, and they find important application in tunable filters, phase shifters, and tunable resonators. These resonators are also extensively used for material characterization applications. The resonance frequencies of these sensors are mainly dependent on the unit cell structural parameters of the resonator. Several resonators can be employed for multi-band operation along a microstrip line. In [11], multiple resonators are coupled from the transmission line along the horizontal axis of the sensor, which increases the overall size of the sensor.

Conventional structures like the ring resonator, SRR-, CSRR-, and IDC-loaded transmission line-based resonant structures have been frequently utilized for material testing and sensor applications [14,15]. The substantial electric field concentration gives the CSRR-loaded RF sensors good sensitivity to the test object. For the testing of materials, several types of CSRR/SRR-based sensors have been suggested [12,14,15]. The CSRR-based sensor has a transmission notch only at a designed fixed frequency. The required set of dimensions needs be changed to change the resonance frequency. In accordance with the device design and operation mode, a variety of resonance frequencies have been used along its length as well as the height of the structure.

For dual-band operation, most reported RF sensors are designed by using single-element- [14,16,17] or multi-resonator-designed sensors [11]. For material characterization at multi-frequencies, the main drawback of multiple resonator planar sensors is that their overall size is increased. Recently, it has become possible to design reconfigurable structures with increased tuning capability by using a varactor diode. These structures contribute to the reduction in the size of microwave structures by being merely fractions of the operational wavelength in size.

Varactor diodes are a suitable candidate to make these structures tunable for overcoming the drawbacks of increased size, mutual coupling, and time-consuming testing methods. The majority of the varactor-loaded sensors in published works use a pair of CSRRs and SRRs to achieve the desired tuning range while maintaining a suitable rejection level in the transmission coefficient. A pair of CSRRs and SRRs together with a biasing arrangement of varactor diodes increases the dimensions and makes the design complicated. Tunable sensors based on a single CSRR for S-band material characterization applications using a varactor diode are proposed [12]. The designed structure became a tunable sensor with relatively low bandwidth tuning and a low notch depth. Another tunable sensor reported employed varactors with an SRR structure or a CSRR structure, which also have a relatively narrow bandwidth and a low transmission notch depth of S_{21} [18].

It can be deduced from the preceding discussion that in order to allow electronic tuning, this resonator can be connected in series to a reversed biased varactor diode. One end of the varactor diode is soldered to microstrip transmission line, and the other terminal can be attached to the resonator structure for achieving tunability. This is why a varactor-diode-based novel resonator has been suggested in this paper. The varactor can be utilized to increase the capacitance connected with the resonator structure by utilizing the suitable reverse-biased voltage. The compact RF sensor based on the varactor-loaded resonator structure described in this work further reduces the influence of mutual coupling, which happens in multi-element resonant systems as discussed above.

The goal of this research is to propose a voltage-tunable simple and compact sensor that is capable of detecting test materials at a wide range of frequencies. In the design process, an initial simulation is performed without tuning the varactor, the S_{21} result shows a resonance frequency around 3.6 GHz, and the resonance is decreased after the addition of a varactor diode in a series of resonators. The microstrip line from the top

layer of the substrate is utilized to excite the sensor. The resonator is etched directly below the microstrip line on the ground plane. The highest retention of energy occurs at the structure’s frequency of resonance, where the accumulated electric and magnetic field magnitudes become equal. The advanced design system (ADS) is utilized to simulate the structure’s equivalent circuit of a tunable resonator structure. When a varactor is added to the structure, the rejection frequency changes with a left-handed wave propagation.

The proposed tunable sensor can perform material testing over a wide measured bandwidth of 1354 MHz using a single metamaterial resonant cell only in the frequency range of 1.79 to 3.15 GHz. S-parameter measurements of various standard substrates are performed, and resonance frequencies are noted to the developed empirical relationship. This characteristic equation of a sensor is used to calculate the dielectric constants of liquid samples at the specified frequency. Using the references of reported data, the calculated values are compared to reported ones. Finally, the performance of the measured sensor is compared with already published results of tunable sensors. The sensing theory and mechanism are given in Section 2, the sensor 3D design and circuit simulations are explained in Section 3 and parametric analysis is completed in Section 4. Measurement results are explained in Section 5 with simulated, measured and calculated results compared, which is followed by a discussion. Finally, the conclusion is drawn and applications are stated in Section 6.

2. Theory and Analysis

The miniaturization of microwave circuits can be achieved by metamaterial resonant structures because the size of metamaterial resonators are only fractions of the wavelength of operation. These structures can be excited by transmission lines like the MTL or a co-planar waveguide with ground (CPWG) from the top of the substrate. A metamaterial resonator is engraved in the ground plane just below these transmission lines. These electrically small size resonators like ring, split ring and CSRRs makes them ideal for realization of compact circuits like sensors and filters, etc. The addition of the tunable capacitance of a varactor diode along with the resonator’s capacitance makes it ideally suitable option to realize tunable sensors.

Additional capacitance of the material under test (MUT) placed on top of the sensor perturbs the electromagnetic fields distribution of the resonator. So, the sensor’s resonance frequency will be shifted toward the low-frequency spectrum depending upon dielectric constant ϵ_r of the subject MUT. The relationship between the relative resonance frequency shift and the dielectric properties of permittivity and permeability of MUT is given by:

$$\frac{\Delta f_r}{f_r} = \frac{\int_v (\Delta\epsilon \vec{E}_1 \cdot \vec{E}_0 + \Delta\mu \vec{H}_1 \cdot \vec{H}_0) \partial v}{\int_v (\epsilon_0 \cdot |\vec{E}_0|^2 + \mu_0 \cdot |\vec{H}_0|^2) \partial v} \tag{1}$$

While the resonance frequency of the subject resonator is given by:

$$f_r = \frac{1}{2\pi(L_r(C_r + C_m))} \tag{2}$$

Any change in resonant frequency can be observed by progressively changing the applied voltage to validate the tunability of these sensors. The behavior of the varactor diode is to decrease the capacitance as applied voltage is increased, so in turn, the result is an increase in the sensor’s resonance frequency. Around the frequency of resonance, these sensors show negative values of real permittivity (ϵ_r) and permeability (μ_r). Another evidence of their metamaterial behavior [19] is also negative group delay nearby the resonance frequency.

At the resonance frequency of the subject sensor, maximum energy storage takes place, so the stored energies of the electric and magnetic field become equal to each other.

A change of frequency of resonance of resonant structure can be related to the change in the test specimen’s dielectric constant, as given by (3).

$$f_{r,MUT} = f_{r,AIR} \sqrt{\frac{\epsilon_{eff,AIR}}{\epsilon_{eff,MUT}}} \tag{3}$$

The parameters $f_{r,MUT}$ and $f_{r,AIR}$ in (3) are the resonance frequency of the sensor perturbed by MUT and air dielectric, respectively. $\epsilon_{eff,AIR}$ and $\epsilon_{eff,MUT}$ are the effective permittivity of just the sensor only and the effective permittivity of the sensor when a test material is placed on it. Changing the test specimen or changing the subject dielectric can be attributed to changes in the metamaterial sensor’s resonance frequency, and notch depth is affected by the test specimen’s loss tangent. The design of a tunable lightweight dielectric sensor based on a single metamaterial cell is presented in the next section.

3. Sensor Design and Simulation

The fundamental design of the suggested sensor is implemented using a resonator and reverse-biased varactor diode. During the simulation, a varactor diode is considered as the combination of R, L and C elements as suggested by the manufacturer’s datasheet [20]. The equivalent circuit diagram of the suggested sensor is simulated by the use of the ADS circuit simulator. An isometric view of varactor-loaded tunable sensor is depicted in Figure 1a, while a bottom close-up view of the sensor structure is shown in Figure 1b.

For the validation purpose of proposed sensor experimentally, a prototype of the suggested sensor is built on commercially available FR-4 material. A variety of standard solid substrates and liquid samples are measured ultimately for obtaining S-parameters. The resonance frequencies are noted and are used for obtaining the value of the dielectric constant in the required frequency range by the presented empirical characteristic formula shown in next sections.

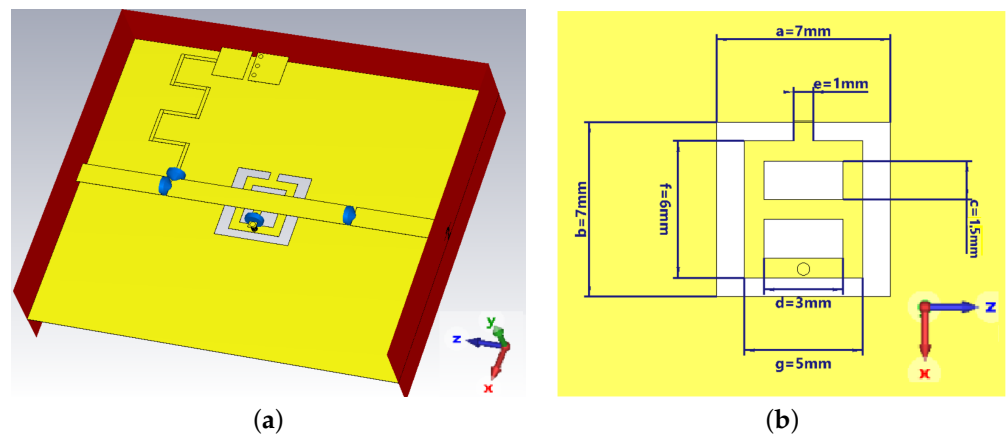


Figure 1. (a) Isometric view of varactor-loaded tunable sensor, (b) Bottom close-up view of sensor structure.

The fixed resonator-based sensor can create transmission minima only at a particular operating frequency. To adjust the resonance frequencies, the tuning parameters must be adjusted with the resonator’s frequency of resonance. This issue can be handled by creating an adequate tuning circuit with a varactor diode and the proper biasing configuration. A rise in diode capacitance lowers the frequency of resonance, thereby rendering the sensor adjustable. DC bypass capacitors are used in the DC feed network to decouple the DC from the network analyzer, and a quarter-wave RF bypass line is implemented for an optimum operating frequency of 2 GHz.

In contrast to already reported structures that used pairs of varactor-loaded CSRRs, the proposed structure utilizes a single resonator and varactor diode to attain the compact design. The suggested sensor is small in size and is made of FR-4, which is a widely

accessible commercial material. The PCB has a height of 0.8 mm with both sides using 17 μm of copper. The overall dimensions of the sensor measures $W \times L \times h$ 25 by 35 mm by 0.8 mm. Dimensions of the sensor PCB and resonant structure are listed in Table 1. The top of the sensor has the microstrip line etched in it with the varactor diode in exact center of the sensor PCB and resonator also. By adjusting the applied voltage across the tunable varactor diode, we can electronically modify the sensor’s electrical properties like the resonance frequency and in turn group delay also. This metamaterial’s negative permittivity along with the addition of tunable capacitance is responsible for the tunable rejection band present in the S_{21} results.

Table 1. Structural parameters of the proposed sensor.

Parameter	Value (mm)	Parameter	Value (mm)
Epsilon r	4.3	Copper Height	0.017
Substrate Length	35	Substrate Width	30
Substrate Height	0.8	Line Width of $\lambda/4$	0.34
Trace Width	1.9	Length of $\lambda/4$	21.8
a	7	b	7
c	1.5	d	3
e	1	f	6
g	5	Via Dia	0.4

3.1. Three-Dimensional (3D) Structure Simulation

The top view of the proposed tunable sensor is depicted in Figure 2. In the developed structure, the tunable varactor is attached at one end to the microstrip line and at the other end to the resonator through via. A DC is fed to the varactor diode via a quarter-wave thin line with an additional inductor attached to the microstrip line that serves as an RF choke. The cathode terminal of the varactor is attached to the microstrip line, and the anode of the varactor is connected to a resonator etched in the ground plane by a metallic via. RF chokes and DC block capacitors are placed in the appropriate positions to properly isolate DC and RF signals. The DC line is meandered to reduce the size of the sensor, while the inductor in the DC path is for the additional isolation of RF and DC signals.

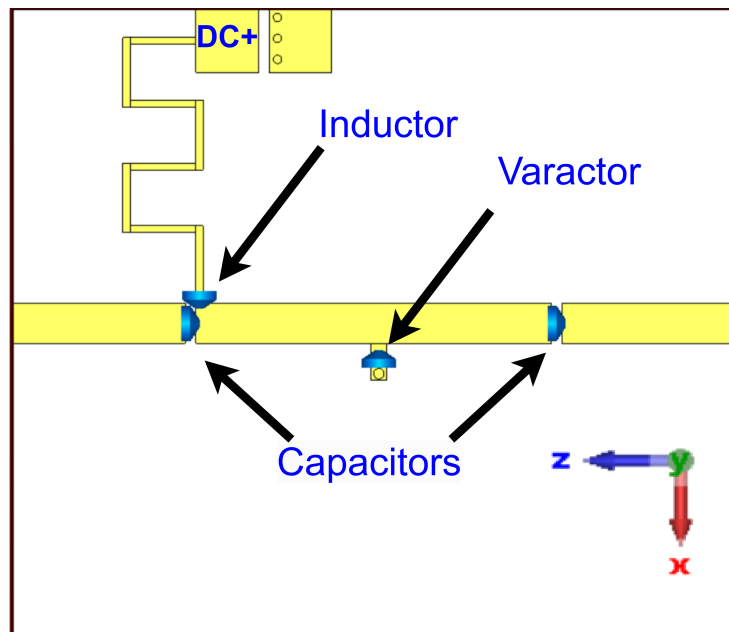


Figure 2. Top view of sensor with varactor and DC feed network.

First, simulation is carried out by using MTL coupled with a resonator only. Resonance frequency is shifted toward the lower side from 3.6 to 3.1 GHz because of the addition of capacitance added by the varactor diode. Simulated results with and without the varactor are shown in Figure 3. The proposed tunable sensor is a series combination of modified rectangular resonator and tunable capacitance diodes. This modified rectangular resonator has a horizontal line joining its arms. The results of the 3D solver simulation and the circuit model simulation show good agreement.

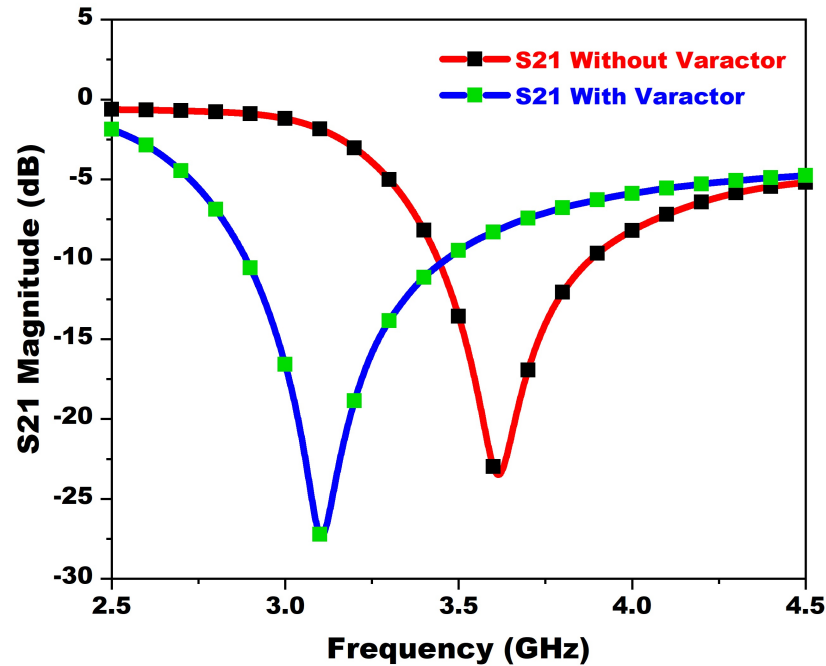


Figure 3. S_{21} simulation results of sensor with and without tuning varactor.

3.2. Sensor's Equivalent Circuit

The proposed resonator's circuit model is exactly like the one depicted in Figure 4a, which is a parallel combination of L_r , C_r , and R_r . The proposed sensor's equivalent circuit is simulated using the ADS circuit simulator. The equivalent circuit MTL has series DC bypass capacitors and a shunt inductor with a quarter-wave line for DC injection into the varactor diode. The tunable varactor diode is in series combination with the resonator and ultimately connected to the ground plane.

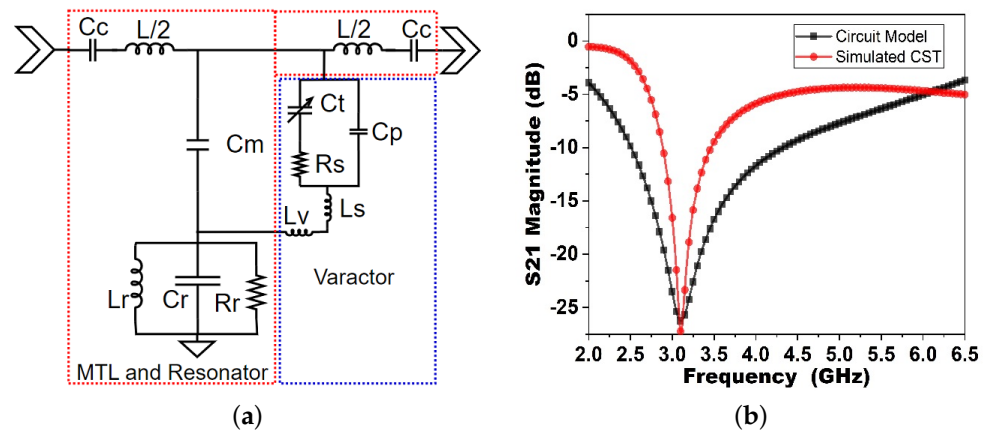


Figure 4. (a) Equivalent circuit of MTL, resonator and varactor, (b) comparison of circuit model and 3D simulation.

Using the approach described in [15], the equivalent circuit parameters C_r , L_r , and R_r are determined to be 0.6765 pF, 0.699 nH and 1342 Ohms. L is 3.7 nH and C_m is 2.41 pF. For reverse voltages ranging from 0 to 20 V, the capacitance of SMV2201-040LF is 2.1 and 0.23 pF, respectively. A comprehensive table of symbols and abbreviations is given in Appendix A, Table A1. The SPICE model of the tuning varactor (SMV2201) diode is depicted in a red box in Figure 4a, and the corresponding model parameters are reported in Table 2. A comparison of 3D full-wave simulation and ADS simulation of the equivalent circuit shown in Figure 4b has very good agreement.

Table 2. Equivalent circuit values of sensor circuit.

Parameter	Value	Parameter	Value
C_c	10 pF	L_s	0.45 nH
C_m	2.4184 pF	L_r	0.699 nH
C_p	0.075 pF	L_v	0.375 nH
C_r	0.6765 pF	R_s	5.41 Ω
C_t	0.23 pF	R_r	1342 Ω
L	3.7 nH	V_s	0–20 V

4. Parametric Analysis

Parametric analysis is completed by changing one parameter and others to remain at their initial value. The reason is to minimize impact on other parameters while one parameter is changed. During simulation, it is observed that increasing the dimensions of the resonator causes the resonance frequency to shifting toward lower frequencies. As mentioned in the theory and analysis section, group delay simulation of the sensor can verify its metamaterial behavior. So, the sensor’s group delay with Air MUT from 1.762 to 3.105 GHz is simulated by by changing V_s from 0 to 20 V, as depicted in Figure 5.

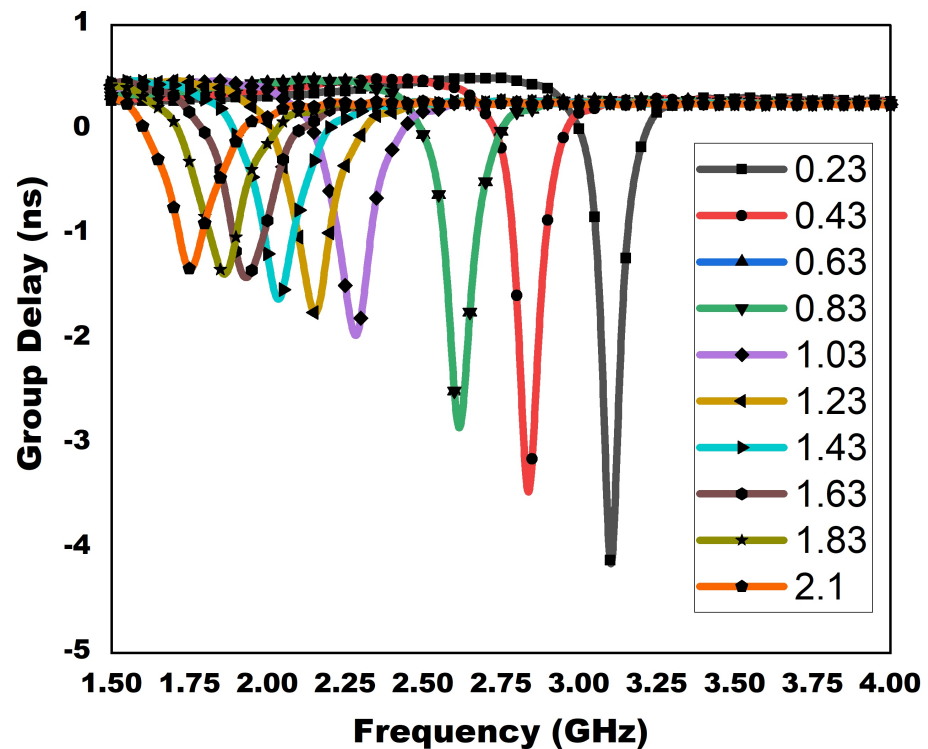


Figure 5. Group delay simulation of sensor with Air MUT from 1.762 to 3.105 GHz by changing $V_s = 0$ to 20 V.

Metamaterial properties are verified by group delay simulation in CST simulation results at ten values of tunable capacitance ($C_t = 0.23\text{--}2.1$ pF) shown in Figure 6a. The curve-fitting method is used to obtain the relationship of diode capacitance to the resonance frequency of the unloaded sensor, as shown in Figure 6b, which is obtained by the model of this sensor given in (4).

$$F_r = 3.3712 - 1.3323 \times C_t(\text{pF}) + 0.2746 \times C_t^2(\text{pF}) \quad (4)$$

The gap between MTL and via to the ground plane is placed to allow for the soldering of the varactor diode. This also caused a shift toward lower frequency due to additional inductance of the via hole. The increase in the width of the connection line between MTL and the via hole can shift the resonance frequency toward a lower frequency due to increased capacitance. We set the diameter of via as 0.4 mm to have minimum impact on the frequency of the resonance behavior. There are two possibilities during the integration of a varactor with a unit metamaterial cell. One is a parallel combination of the resonator and varactor, and the second one is a series combination of the resonator with a microstrip line.

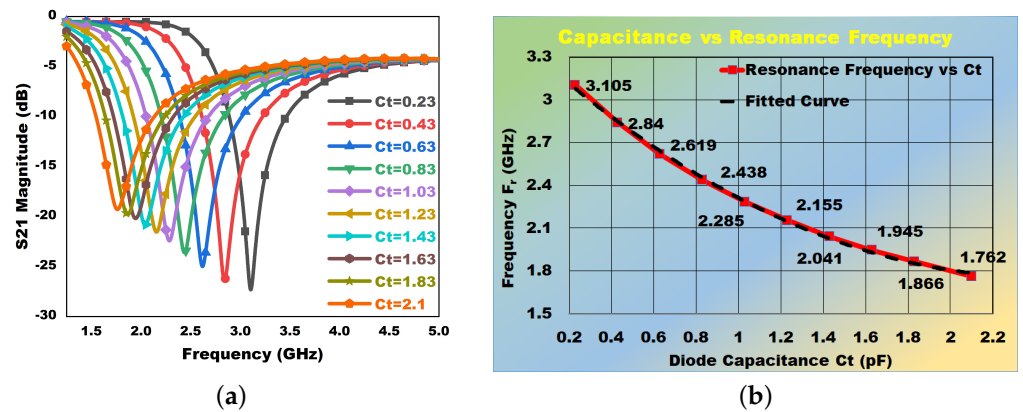


Figure 6. (a) Simulation results of sensor by tuning ‘ C_t ’, (b) Resonance frequency vs. capacitance ‘ C_t ’ of sensor with ‘Air MUT’.

4.1. E-Field Analysis

For understanding the sensing phenomenon, the absolute maximum E-field of the sensor with Air MUT at 1.762 GHz is plotted in Figure 7a. As there is a minima in S_{21} at the lower frequency for $V_s = 0$ or $C_t = 2.1$ pF, there is almost null transmission of signal. Wave propagation in case of the upper bound of the usable sensor frequency is simulated as 3.105 GHz, so the E-field of the sensor with Air MUT is also simulated at 3.105 GHz, as shown in Figure 7b. Both of these E-field results show nearly identical response, which confirms the transmission notch after tuning of the sensor from lower to higher-end frequencies.

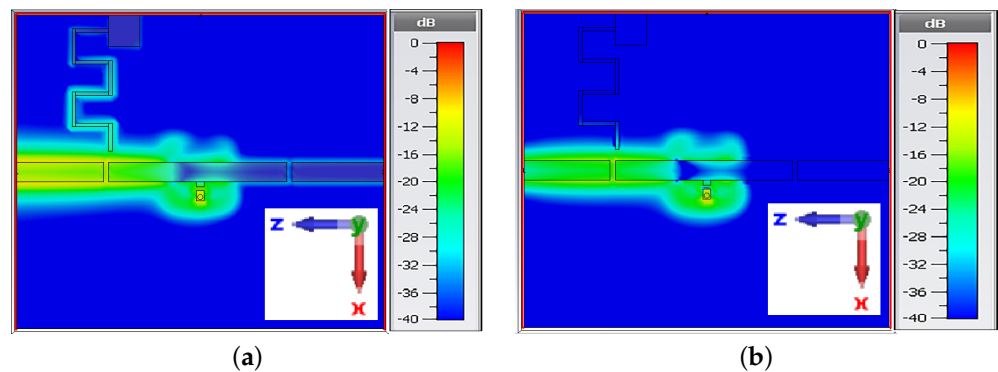


Figure 7. (a) E-field of sensor with Air MUT at 1.762 GHz, (b) E-field of sensor with Air MUT at 3.105 GHz.

4.2. Air Gap Analysis

Air gap analysis is performed, and the effect on resonance frequency is studied for the case of solid MUTs only because the air gap is absent in case of oil samples. Its effect is to increase the resonance frequency up to the value directly proportional to the height of the air gap. In this case, capacitance is kept constant and RT/Duroid 6010.2 is chosen, MUT having the highest dielectric constant of 10.7 among commercial substrates. The change in resonance frequency can be adjusted by slightly adjusting the diode’s voltage to nullify the air gap effect.

4.3. Loss Tangent

For obtaining complex permittivity, the loss tangent is also required apart from the dielectric constant value. Loss tangent simulation is performed by increasing loss tangent values, and the results are plotted in Figure 8. A mathematical relationship of loss tangent relating the notch depth of the perturbed MUT is obtained using the curve-fitting method, as given by Equation (5).

$$\tan D = 1.08596 + 0.0703 \times S_{21}(\text{dB}) + 0.0011 \times (S_{21}(\text{dB}))^2 \tag{5}$$

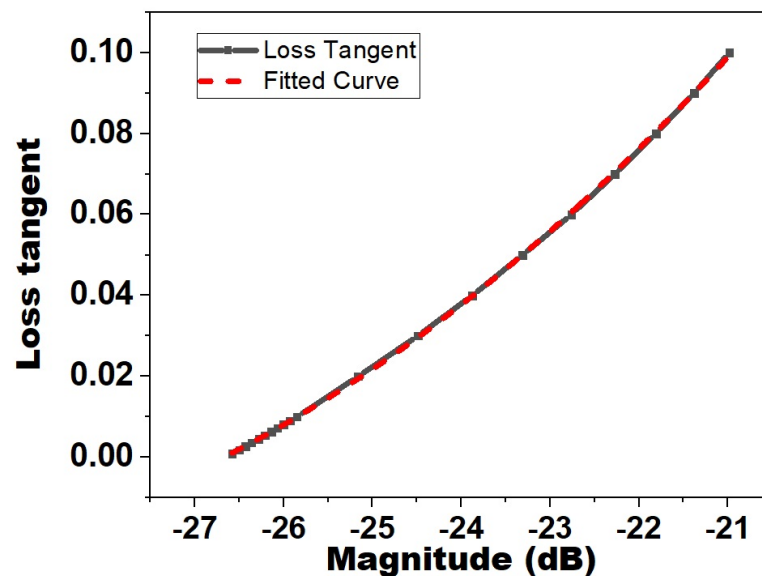


Figure 8. Relationship of notch depth ($S_{21}(\text{dB})$) with loss tangent.

5. Measurement and Discussion

The prototype of the proposed sensor is fabricated for validation of the presented concept. Front and back view dimensions of measurement of the sensor are shown in Figure 9. Components are soldered on the fabricated sensor using SnPb soldering wire; finally, the front and back side view are shown in Figure 10. After careful soldering the required DC bias lumped components, the varactor diode is mounted on the prototype sensor by the normal soldering process. The tunability of the resonance frequency is observed by altering the DC bias voltage from 0 to 20 V.

The ‘air resonance’ frequency of the sensor without the varactor diode is measured as depicted in Figure 11. Measured results very close to the simulated ones are achieved in the frequency range of 1.795 to 3.105 GHz, corresponding to a DC bias of 0 to 20 V. A comparison of simulated and measured results is shown in Figure 12. The measured S-parameter results using SUTs are shown in Figure 13. Figure 14 shows the electric field of a sensor perturbed with LUT, while the setup for the sensor measurements is shown in Figure 15. Measured results in case of SUTs are used to form the empirical relationship between the dielectric constant of MUT and the resonance frequency (6). After that, the resonance frequency values of the oil samples are used to calculate their respective dielectric constants.

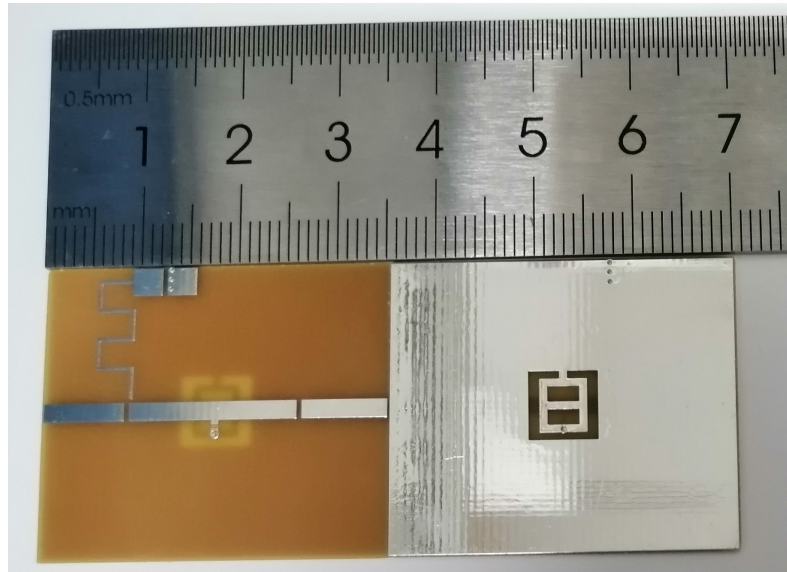


Figure 9. Measurement of sensor dimensions: front and back view.

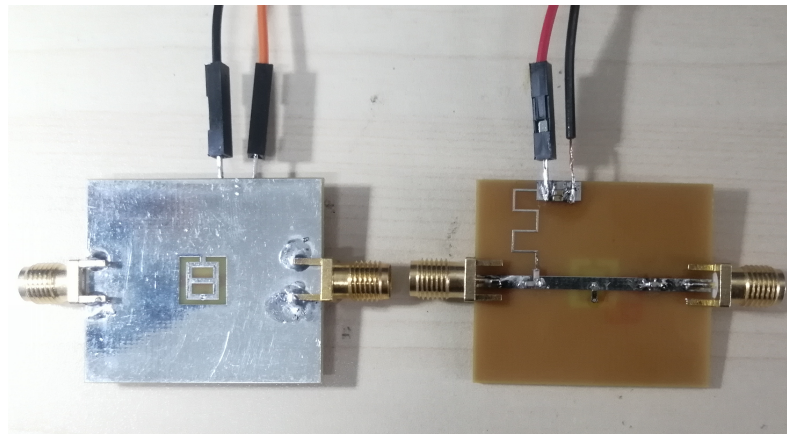


Figure 10. Fabricated sensor front and back side.



Figure 11. Measurement setup of sensor using Agilent's E8363B Network Analyzer.

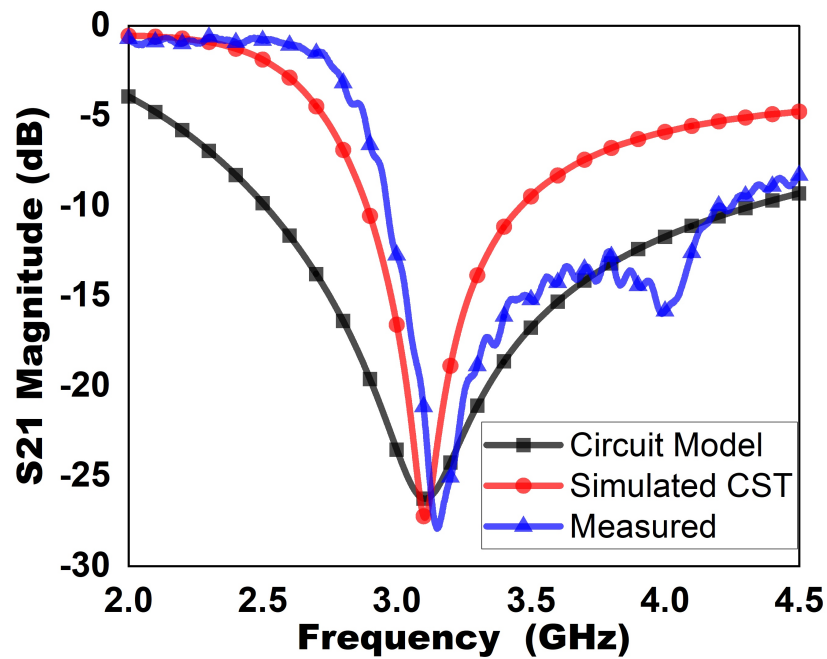


Figure 12. Comparison of circuit-simulated, 3D-simulated and measured results of bare sensor for $V_s = 20$ V.

5.1. Solid Dielectric Measurements

First, Rogers© RT5880, RO4350B and RO4003C substrates are used to perform solid dielectric measurements. The measured results of these SUTs are used to derive Equation (6) by using the procedure reported in [15]. Solid dielectric measurements are performed by using substrate samples of 0.51 mm height. The sensor’s S-parameter measured results using standard substrates are shown in Figure 13. The standard SUT’s calculated dielectric constant results are in good agreement with the simulated ones and are shown in tabular form in Table 3.

$$\epsilon'_r = \frac{0.08138 - \sqrt{0.006623 - 0.02092(3.1516 - f_{r,MUT})}}{0.01046} + 1 \tag{6}$$

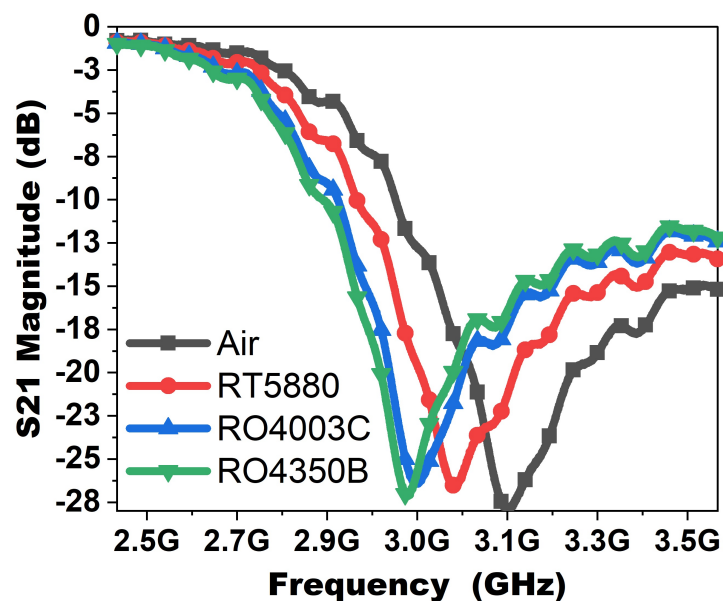


Figure 13. Measured results of SUTs using sensor with network analyzer at $V_s = 20$ V.

Table 3. Comparison of dielectric measurements of standard substrates.

SUTs	Resonance Frequency (GHz)		Dielectric Constant (ϵ_r)	
	Simulated	Measured	Calculated	Reported
Air (f_0)	3.105	3.1516	1	1.00059
RT5880	2.983	3.0614	2.201	2.2
RO4003C	2.874	2.9962	3.22	3.38
RO4350B	2.866	2.9816	3.486	3.48

The difference between the simulation values of resonant frequencies and those obtained from measurements can be attributed to the non-ideal behavior of substrates and components involved in the fabrication of the proposed sensor. During the manufacturing process, tolerances of the PCB fabrication can directly affect the resonant frequency along with external reflections also during the test process. Components' tolerances like that of the varactor diode, DC block capacitors and the small fluctuations in power supply noise can overall affect the differences in the measured and simulated results.

5.2. Liquid Dielectric Measurements

Liquid dielectric measurements are performed by installing a cylindrical liquid container having a height of 4 mm just outside the tunable resonator. First, a measurement of air container resonance frequency is made and recorded. This resonance frequency and other resonances are recorded in the measurement of certain available oil samples. From these values, the calculated dielectric constant of oil samples is computed by using Equation (6).

As the volume of the LUT is increased, it results in an increase of the material height so the the perturbed resonance frequency is decreased [9,21]. This decrease in the resonance frequency due to the increase in the volume of the sample (or height of LUT in the container) shows the effect as the increase in dielectric constant, virtually. Ultimately, after using the sample LUT height of 3 mm, the decrease in the resonance frequency is almost negligible; this height is used to assess the dielectric constant of all sample LUTs. Simulation of the electric field is performed, and the maximum value is obtained at the interface of the resonator structure and liquid sample, as shown in Figure 14a. Simulated electric field penetration inside the liquid oil sample is shown in Figure 14b.

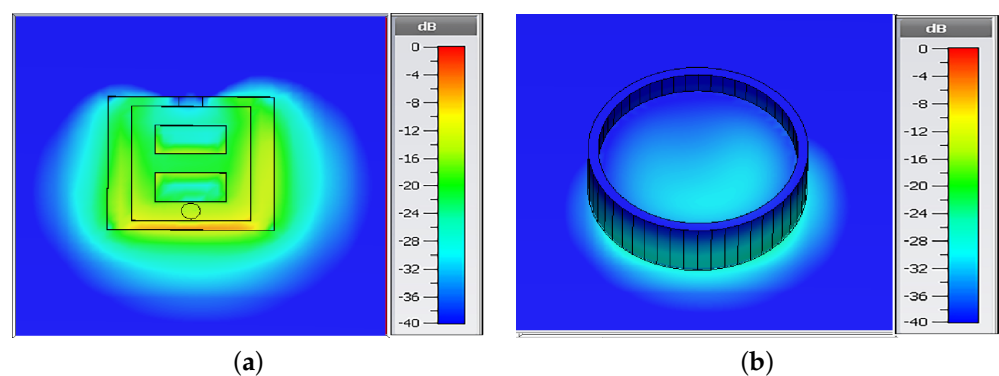


Figure 14. (a) E-field of LUT perturbed sensor with sample hidden, (b) electric field penetration inside liquid oil sample.

Oil samples are poured in the mentioned cylindrical container mounted outside the sensing area one by one, as shown in Figure 15. After each oil sample measurement, the sensing area is cleaned by alcohol, and the air resonance frequency is verified. The sensor's S-parameter measured results of commercially available oil samples are shown in Figure 16. Almond, sunflower, olive and coconut oils are measured and the results are recorded. The liquid specimen oil sample's measured and calculated results also have close values to

those in the reported literature, as Table 4 shows. As evident from these measurements, the cylindrical container has a negligible effect on the air resonance frequency.

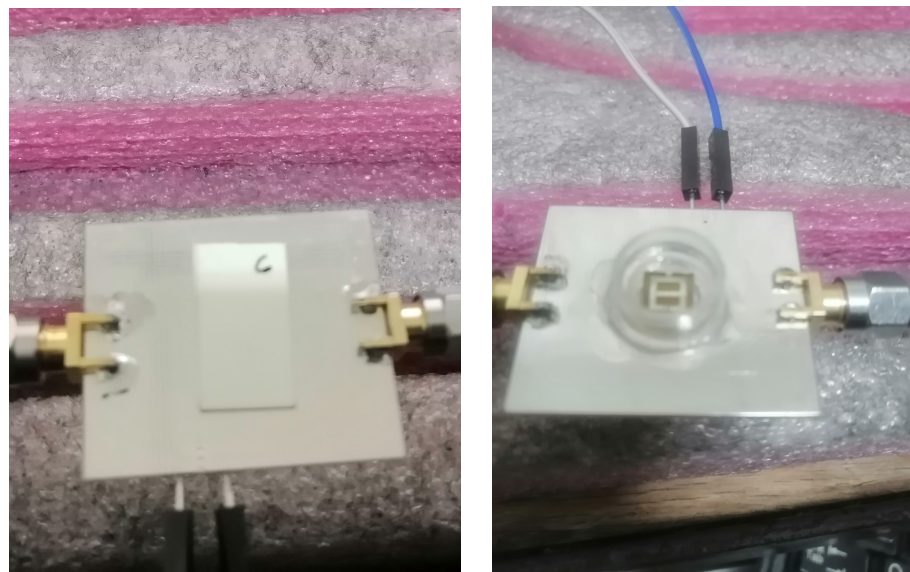


Figure 15. Dielectric measurements of solids (SUTs) and liquids (oil LUTs).

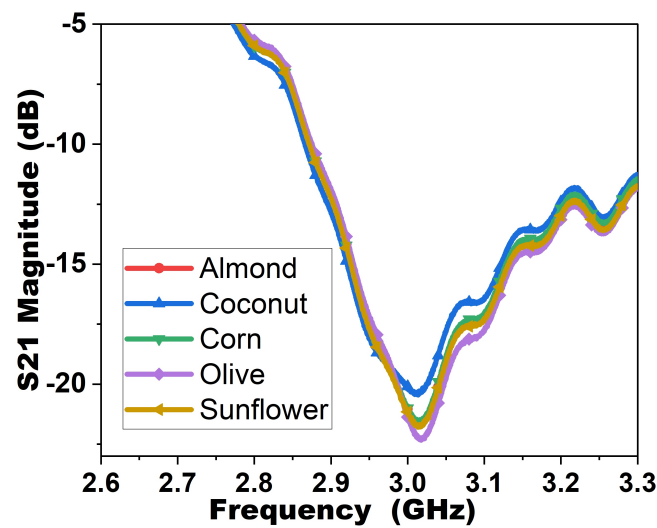


Figure 16. Measured results of sensor in case of oil samples for $V_s = 20$ V.

Table 4. Dielectric measurements of oil samples.

Oil Samples	Measured Resonance Frequency (GHz)	Dielectric Constant (ϵ_r)	
		Calculated	Reported
Air container	3.1506	1.01	1.00059
Almond	3.015	3.05	3.03
Olive	3.0176	3.00	3.08
Sunflower	3.0136	3.08	3.11
Coconut	3.013	3.09	3.12

5.3. Multi-Element Composite Sensor

The current work is focused on conducting measurements in the L and S-band; for other frequencies, a multi-element composite sensor is a viable option. Sensors having

frequency bands to cover the broadband spectrum from 3.15 to 13 GHz can be designed using this configuration. A reference system is reported in [22], but it uses a manual tuning of components. In our scheme, these sensors can be tuned electronically, sensors are combined in parallel to each other, and measurements are taken one sensor at a time, but the setup does not need to be changed. A parallel combination is implemented by using RF switches at the input and output of these sensors. This system becomes a multi-sensor network for dielectric constant measurement in a wideband spectrum range.

6. Performance Comparison

The comparison of the measured sensor’s performance in case of SUT’s with the literature reported results are shown in Table 3. These results show that the simulated, measured and calculated dielectric constant of solid SUTs are very close to each other. The measured S-parameter results of the perturbed sensor with liquid oil samples are shown in Figure 16. The already reported tunable structures are analyzed in terms of bandwidth, frequency range, applied tuning voltage and type of application. The proposed sensor is significant in terms of giving insight as a new structure of tunable sensors.

Various applications of varactor-loaded structures include tunable circuits using varactor-loaded transmission lines (TLs) and permittivity sensors for solid and liquid materials. The S-band tunable sensor of solids and liquids [12] shows a notch depth of approximately −15 dB, while the proposed measured sensor has a relatively deeper notch depth of −17 to −24 dB for various tuning voltages. A performance comparison of the proposed sensor with the reported literature sensor’s measured results are shown in Table 5. This comparison shows that the proposed tunable sensor exhibits a broader tunable bandwidth using a relatively low voltage range. So, a varactor diode can be used to change the capacitance associated with the resonant structure, thus making it tunable by using applying appropriate reverse bias voltage.

Table 5. Performance comparison with studies reported in the literature.

Reference No.	Frequency (GHz)	Tunable (Bandwidth)	Tuning Voltage	Application Type
[14]	4.76 and 112	Dual frequency	–	Sensor (Solids)
[23]	3.65 and 7.38	Dual frequency	–	Sensor (Liquids)
[18]	0.5–1	Yes (500 MHz)	0–28 V	Tunable TL
[19]	1.25–1.85	Yes (600 MHz)	0–14 V	Tunable TL
[13]	0.83–1.58	Yes (750 MHz)	0–36 V	Dielectric Sensor
[12]	2.7–3.1	Yes (400 MHz)	0–28 V	Sensor Solids and Liquids
This Work	1.795–3.1504	Yes (1354 MHz)	0–20 V	Sensor Solids and Liquids

Related Work

This work has proposed a different sensor structure from other related sensors which have mostly SIW, SRR and CSRR structures [24–27]. Related work of dielectric constant sensors is shown in Table 6. This tunable sensor solves the unit cell resonators close proximity problem of mutual coupling by tuning resonance frequency achieving multi-frequency operation. Multiple resonators need to be isolated [11] to decrease mutual coupling; thus, they have an increased size, but this is a single metamaterial-based sensor. For multi-resonant elements, the MUT needs to be placed one by one, and the testing process takes a long time due to this multi-resonator geometry. The proposed tunable sensor alleviates this need by changing the test frequency in the tunable bandwidth of 1354 MHz, which is much wider than the previous designs summarized in Table 6. For the

case involving liquid samples, a special sample holder has to be placed on every resonator. The severity of this problem increases for multi-element liquid testing. The proposed sensor also gives a solution to this issue, and once a liquid sample is poured, multi-frequency testing is completed.

The sensors reported in [14,23,28] have resonators to exhibit two fixed resonance frequencies for sensing application, while the passive sensor’s [27] resonance frequency values cannot be changed during measurement. The reported sensor can be tuned to any frequency within the bandwidth using DC voltage, and its resonance frequency can be changed during measurements. This new sensor with series varactor configuration has shown increased bandwidth as compared to previous reported active sensors [12,13,24–26]. So, this single compact resonator design can be applied as an improved wideband tunable sensor in a variety of dielectric measurement applications.

Table 6. Summary of related work.

Reference No.	Type (Active/Passive)	Operating Frequency	Bandwidth	Resonant Element	Application
[28]	Passive	1.3 and 2.6	Dual Band	Dual-band Antenna	Sensor (Liquids)
[26]	Active	2.9 GHz	310 MHz	CSRR	Tunable Sensor
[25]	Active	2.85 GHz	450 MHz	SRR	Tunable TL
[24]	Active	2.8 GHz	800 MHz	CSRR	Sensor (Liquids)
[27]	Passive	5–6 GHz	1000 MHz	SIW	Sensor (Liquids)

7. Conclusions

A planar varactor-loaded tunable sensor for L and S-bands has been demonstrated. The proposed sensor is based on a new resonator in series with a varactor, which allows the testing of a test specimen at multiple frequencies. The proposed design configuration is used to realize a compact sensor, as it does not need multiple resonators for multi-frequency testing. A close matching has been observed between the S-parameters measurements of the unloaded sensor and those obtained using the ADS and CST simulations. A characteristic formula or empirical relationship is presented for the calculation of dielectric constant of solid and liquid test specimen. The applicability of the proposed RF sensor is shown by the closed matching of published data and calculated permittivity results. An enhanced tunable bandwidth of 1.354 GHz in the resonance frequency range from 1.795 to 3.15 GHz can be used for measurement of the solid dielectric materials. The proposed sensor can also act as a biosensor for liquid material characterization. The metamaterial-based tunable resonator design using varactor diodes can also be utilized for various applications in the microwave industry like modulators, phase shifters, filters and oscillators.

Author Contributions: Conceptualization, W.S. and W.H.; methodology, W.S. and Q.A.; software, W.S.; validation, W.S. and G.S.; formal analysis, W.S.; resources, W.H.; writing W.S. and Q.A. original draft preparation, W.S. and A.R.B.; review and editing, W.S., A.R.B. and G.S.; supervision, W.H.; project administration, W.H.; funding acquisition, W.H. All authors have read and agreed to the published version of the manuscript.

Funding: This research is funded by the National Science Foundation (NSF 61527805).

Data Availability Statement: The data presented in this research are available on reasonable request.

Acknowledgments: The authors would like to thank Vahid Rastinasab, Huan Yu and Liu Qing Guo for their support in this work.

Conflicts of Interest: The authors declare no conflicts of interest.

Appendix A

Abbreviations, variables and symbols used in this article are listed in Table A1.

Table A1. Table of variables and symbols.

Variable	Description	Variable	Description
ϵ_r	Relative dielectric constant	tanD	Tangent delta or loss tangent
MTL	Microstrip transmission line	Fr	Sensor's resonance frequency
a	Width of ground plane cut	b	Length of ground plane cut
c	Vertical gap between arms	d	Horizontal gap between arms
e	Width of connecting slit	f	Length of resonator arms
g	Width of resonator arms	Via Dia.	Connecting via diameter
Cc	DC decoupling capacitor	Ls	Series inductance DC to MTL
Cm	Mutual capacitance MTL and resonator	Lr	Resonator inductance
Cp	Varactor parallel capacitance	Lv	Via inductance
Cr	Resonator capacitance	Rs	Varactor series resistance
Ct	Varactor tunable capacitance	Rr	Resonator resistance
L	MTL inductance	Vs	Varactor tunable voltage

References

- Cao, Y.; Ruan, C.; Chen, K.; Zhang, X. Research on a high-sensitivity asymmetric metamaterial structure and its application as microwave sensor. *Sci. Rep.* **2022**, *12*, 1255. [[CrossRef](#)] [[PubMed](#)]
- Lammert, V.; Heine, C.; Wessel, J.; Jamal, F.I.; Kissinger, D.; Geiselbrechtinger, A.; Issakov, V. A K-band complex permittivity sensor for biomedical applications in 130-nm SiGe BiCMOS. *IEEE Trans. Circuits Syst. II Express Briefs* **2019**, *66*, 1628–1632. [[CrossRef](#)]
- Qureshi, S.A.; Zainal Abidin, Z.; Isa Ashyap, A.Y.; Majid, H.A.; Kamarudin, M.R.; Yue, M.; Zulkipli, M.S.; Nebhen, J. Millimetre-wave metamaterial-based sensor for characterisation of cooking oils. *Int. J. Antennas Propag.* **2021**, *2021*, 5520268. [[CrossRef](#)]
- Alimenti, A.; Pittella, E.; Torokhtii, K.; Pompeo, N.; Piuze, E.; Silva, E. A Dielectric Loaded Resonator for the Measurement of the Complex Permittivity of Dielectric Substrates. *IEEE Trans. Instrum. Meas.* **2023**, *72*, 1–9. [[CrossRef](#)]
- Jha, A.K.; Akhtar, M.J. A Generalized Rectangular Cavity Approach for Determination of Complex Permittivity of Materials. *IEEE Trans. Instrum. Meas.* **2014**, *63*, 2632–2641. [[CrossRef](#)]
- Yaw, K.C. Measurement of dielectric material properties. *Appl. Note Rohde Schwarz*. **2012**, 1–35.
- Esfandiyari, M.; Lalbakhsh, A.; Jarchi, S.; Ghaffari-Miab, M.; Mahtaj, H.N.; Simorangkir, R.B. Tunable terahertz filter/antenna-sensor using graphene-based metamaterials. *Mater. Des.* **2022**, *220*, 110855. [[CrossRef](#)]
- Majidifar, S.; Karimi, G. New approach for dielectric constant detection using a microstrip sensor. *Measurement* **2016**, *93*, 310–314. [[CrossRef](#)]
- Lee, C.S.; Bai, B.; Song, Q.R.; Wang, Z.Q.; Li, G.F. Open complementary split-ring resonator sensor for dropping-based liquid dielectric characterization. *IEEE Sens. J.* **2019**, *19*, 11880–11890.
- Lee, H.J.; Lee, H.S.; Yoo, K.H.; Yook, J.G. DNA sensing using split-ring resonator alone at microwave regime. *J. Appl. Phys.* **2010**, *108*, 014908. [[CrossRef](#)]
- Ansari, M.A.H.; Jha, A.K.; Akhter, Z.; Akhtar, M.J. Multi-Band RF Planar Sensor Using Complementary Split Ring Resonator for Testing of Dielectric Materials. *IEEE Sens. J.* **2018**, *18*, 6596–6606. [[CrossRef](#)]
- Tiwari, N.K.; Tiwari, Y.; Akhtar, M.J. Design of CSRR-Based Electronically Tunable Compact RF Sensor for Material Testing. *IEEE Sens. J.* **2018**, *18*, 7450–7457. [[CrossRef](#)]
- Sam, S.; Lim, S. Ultra-wideband tunable resonator based on varactor-loaded complementary split-ring resonators on a substrate-integrated waveguide for microwave sensor applications [Letters]. *IEEE Trans. Ultrason. Ferroelectr. Freq. Control* **2013**, *60*, 657–660. [[CrossRef](#)] [[PubMed](#)]
- Xiao, H.; Yan, S.; Guo, C.; Chen, J. A Dual-Scale CSRRs-Based Sensor for Dielectric Characterization of Solid Materials. *IEEE Sens. Lett.* **2022**, *6*, 1–4.
- Shahzad, W.; Hu, W.; Ali, Q.; Raza, H.; Abbas, S.M.; Lighthart, L.P. A Low-cost metamaterial sensor based on DS-CSRR for material characterization applications. *Sensors* **2022**, *22*, 2000. [[CrossRef](#)]
- Zhang, X.; Ruan, C.; Cao, Y. A dual-mode microwave sensor for edible oil characterization using magnetic-LC Resonators. *Sens. Actuators A Phys.* **2022**, *333*, 113275. [[CrossRef](#)]
- Armghan, A.; Alanazi, T.M.; Altaf, A.; Haq, T. Characterization of dielectric substrates using dual band microwave sensor. *IEEE Access* **2021**, *9*, 62779–62787.
- Velez, A.; Bonache, J.; Martin, F. Varactor-Loaded Complementary Split Ring Resonators (VLCSRR) and Their Application to Tunable Metamaterial Transmission Lines. *IEEE Microw. Wirel. Components Lett.* **2008**, *18*, 28–30. [[CrossRef](#)]

19. Nesimoglu, T.; Sabah, C. A tunable metamaterial resonator using varactor diodes to facilitate the design of reconfigurable microwave circuits. *IEEE Trans. Circuits Syst. II Express Briefs* **2015**, *63*, 89–93. [[CrossRef](#)]
20. Skyworks Solutions, I. SMV2201-SMV2205 Series: Surface Mount, 0402 Silicon Hyperabrupt Tuning Varactor Diodes. Available online: <http://www.skyworksinc.com> (accessed on 25 July 2023).
21. Ansari, M.A.H.; Jha, A.K.; Akhtar, M.J. Design and Application of the CSRR-Based Planar Sensor for Noninvasive Measurement of Complex Permittivity. *IEEE Sens. J.* **2015**, *15*, 7181–7189. [[CrossRef](#)]
22. Cui, Y.; Sun, J.; He, Y.; Wang, Z.; Wang, P. A simple, tunable, and highly sensitive radio-frequency sensor. *Appl. Phys. Lett.* **2013**, *103*, 062906. [[CrossRef](#)] [[PubMed](#)]
23. Kálovics, M.; Iván, K.; Szabó, Z. Microfluidic Mixing Device with Integrated Dual Band Microwave Sensor. *IEEE Sens. J.* **2023**, *23*, 15350–15360. [[CrossRef](#)]
24. Seth, S.; Banerjee, A.; Tiwari, N.K.; Akhtar, M.J. Frequency controlled intelligent standalone RF sensor system for dispersive material testing. *J. Electromagn. Waves Appl.* **2021**, *35*, 1619–1636. [[CrossRef](#)]
25. Gil, I.; Bonache, J.; Garcia-Garcia, J.; Martin, F. Tunable metamaterial transmission lines based on varactor-loaded split-ring resonators. *IEEE Trans. Microw. Theory Tech.* **2006**, *54*, 2665–2674. [[CrossRef](#)]
26. Tiwari, N.K.; Tiwari, Y.; Azad, P.; Akhtar, M.J. Novel design for CSRR based electronically steered compact S-band microwave resonator. In Proceedings of the 2017 IEEE Asia Pacific Microwave Conference (APMC), Kuala Lumpur, Malaysia, 13–16 November 2017; pp. 1238–1241. [[CrossRef](#)]
27. Jafari, F.S.; Ahmadi-Shokouh, J. Reconfigurable microwave SIW sensor based on PBG structure for high accuracy permittivity characterization of industrial liquids. *Sens. Actuators A Phys.* **2018**, *283*, 386–395. [[CrossRef](#)]
28. Zhu, L.; Farhat, M.; Chen, Y.C.; Salama, K.N.; Chen, P.Y. A Compact, Passive Frequency-Hopping Harmonic Sensor Based on a Microfluidic Reconfigurable Dual-Band Antenna. *IEEE Sens. J.* **2020**, *20*, 12495–12503. [[CrossRef](#)]

Disclaimer/Publisher’s Note: The statements, opinions and data contained in all publications are solely those of the individual author(s) and contributor(s) and not of MDPI and/or the editor(s). MDPI and/or the editor(s) disclaim responsibility for any injury to people or property resulting from any ideas, methods, instructions or products referred to in the content.